Inorganic Chemistry
Article

Inorg. Chem. **2009**, *48*, 5983–5995 **5983**
DOI: 10.1021/ic900378d

Luminescent and Magnetic Cyano-Bridged Coordination Polymers Containing 4d−4f Ions: Toward Multifunctional Materials

Elena Chelebaeva,[†,∥] Joulia Larionova,[*,†] Yannick Guari,[†] Rute A. S. Ferreira,[‡] Luis D. Carlos,[*,‡] Filipe A. Almeida Paz,[§] Alexander Trifonov,[∥] and Christian Guérin[†]

[†]*Institut Charles Gerhardt Montpellier, UMR 5253 CNRS-UM2-ENSCM-UM1, Chimie Moléculaire et Organisation du Solide, Université Montpellier II, Place E. Bataillon, 34095 Montpellier cedex 5, France,* [‡]*Departamento de Física and CICECO, Universidade de Aveiro, 3810-193 Aveiro, Portugal,* [§]*Departamento de Química and CICECO, Universidade de Aveiro, 3810-193 Aveiro, Portugal, and* [∥]*G. A. Razuvaev Institute of Organometallic Chemistry of the Russian Academy of Science, Tropinina 49, GSP-44S, 603950, Nizhny Novgorod, Russia*

Received February 25, 2009

A new family of cyano-bridged coordination polymers $Ln(H_2O)_5[M(CN)_8]$ (Ln = Eu, Tb, Sm, Gd; M = Mo, W) were obtained and characterized by X-ray diffraction, photoluminescence spectroscopy, and magnetic analyses. These compounds are isomorphous and crystallize in the tetragonal system *P*4/*nmm*, forming two-dimensional gridlike networks. The Eu- and Tb-containing coordination polymers are room-temperature optically active emitters displaying the characteristic $^5D_0 \rightarrow {}^7F_{0\text{-}4}$ (Eu^{3+}) and $^5D_4 \rightarrow {}^7F_{6-2}$ (Tb^{3+}) transitions. All of the coordination polymers except $Eu(H_2O)_5[M(CN)_8]$ present long-range magnetic ordering at low temperatures. The coexistence of luminescence with ferromagnetic ordering for $Tb(H_2O)_5[M(CN)_8]$ (M = Mo, W) suggests that these compounds may be considered as bifunctional magneto-luminescent coordination polymers exhibiting diverse physical responses when subjected to various external stimuli.

Introduction

Multifunctional materials are a class of materials that combine multiple features including mechanical, electronic, optical, and magnetic properties in a single system and are capable of exhibiting diverse physical responses when subjected to various external conditions. In recent years, multifunctional materials have been at the forefront of current science and technology and are expected to bring important breakthroughs in various technological fields. Traditional multifunctional systems usually include various composite or nanocomposite materials in which one of the components (such as polymers, copolymers, ceramics, or clays) plays the role of the matrix and other components (such as metal ions, nanoparticles, polymers, metal oxides, and others) with various tailored properties are integrated into the matrix.[1] Such composite materials may either present simple coexistence of physical and chemical properties of components or exhibit novel properties due to the mutual interaction between the two individual components. In this respect, numerous multifunctional composite materials in which the two components are dispersed within each other or covalently linked have been synthesized during the past 20 years.[2] One of the new interesting ways to achieve unusual multifunctional materials is the synthesis of molecule-based materials which combine two or more physical properties in the same crystal lattice.[3] For this reason, the research activity in this field has increased in the past 10 years, and several multifunctional coordination polymers combining magnetic properties and optical activity,[4] magnetic and nonlinear

*To whom correspondence should be addressed. Fax: (33) 4 67 14 38 52 (J.L.), (351) 234 378 197. E-mail: joulia.larionova@univ-montp2.fr, lcarlos@ua.pt (L.D.C.).

(1) (a) Gomez-Romero, P.; Sanchez, C. *Functional Hybrids Materials*; Wiley-VCH Verlag GmbH & Co. KgaA: Weinheim, Germany, 2004. (b) Weigert, E. C.; South, J.; Rykov, S. A.; Chen, J. G. Catal. Today 2005, 99, 285–290. (c) Galán-Mascarós, J.R.; Coronado, E. C.R.Chimie 2008, 11, 1110–1116. (d) Torquato, S.; Hyun, S.; Donev, A. Phys. Rev. Lett. 2002, 89, 266601.

(2) (a) Torquato, S. *Random Heteroheneous Materials: Microstructure and Macroscopic Properties*, Springer-Verlag, New-York, 2002; (b) Rabu, P.; Drillon, M. Adv. Eng. Mater. 2003, 5, 189. (c) Coe, B.J.; Curati, N.R. Comm. Inorg. Chem. 2004, 25, 147. (d) Knutson, J.I.; Martin, D.J.; Mitzi, D.B. Inorg. Chem. 2005, 44, 4699. (e) Gruselle, M.; Train, C.; Boubekeur, K.; Gredin, P.; Ovanesyan, N. Coord. Chem.Rev. 2006, 250, 2491.

(3) (a) Maspoch, D.; Ruiz-Molina, D.; Veciana, J. *Chem. Soc. Rev.* **2007**, *36*, 770. (b) Gaspar, A. B.; Ksenofontov, V.; Seredyuk, M.; Guetlich, P. *Coord. Chem. Rev.* **2005**, *249*, 2661. (c) Coronado, R.; Galan-Mascaros, J. R.; Romero, F. *Funct. Hybrid Mater.* **2004**, 37 and references therein.

(4) (a) Rikken, G. L.; Raupach, E. *Nature* **2000**, *405*, 932. (b) Minguet, M.; Luneau, D.; Lhotel, E.; Villar, V.; Paulsen, C.; Amabilino, D. B.; Veciana, J. *Angew. Chem. Int. Ed.* **2002**, *41*, 586. (c) Kumagai, H.; Inoue, K. *Angew. Chem. Int. Ed.* **1999**, *38*, 1601. (d) Barron, L. D. *Nature* **2000**, *504*, 895. (e) Yamaguchi, I.; Fujinaga, E.; Ozeki, T.; Yamamoto, T. *Bull. Chem. Soc. Jpn.* **2004**, *77*, 1773–1782.

Published on Web 06/05/2009

optical properties,[5] porosity and optical or magnetic properties,[6] or conductivity and magnetic properties[7] have been reported. On the other hand, analogous efforts regarding multifunctional coordination polymers combining magnetism and luminescence have been comparatively fewer.[8−11] These compounds mainly belong to two types of coordination polymers: (i) inorganic−organic hybrid materials based on luminescent trivalent lanthanides ions (Ln^{3+}) assembled into two- or three-dimensional networks by using various multicarboxylate ligands,[8] usually presenting typical Ln^{3+} luminescent properties and weak antiferromagnetic interactions between the ions without magnetic ordering, or (ii) hybrid host−guest compounds in which luminescent cations are intercalated between magnetic layers assembled from transition metal ions.[9] However, due to the difficulty in the host−guest components' compatibility, only a few molecule-based networks presenting a true coexistence of magnetic ordering and luminescence properties have been reported.[9a]

Recently, we reported preliminary results of a promising way to achieve bifunctional luminescent molecule-based magnets by designing $Tb(H_2O)_5[Mo(CN)_8]$ in which luminescent Tb^{3+} ions were associated with cyanomalybdate building blocks in a two-dimensional network.[10] This compound presents the characteristic luminescence of the Tb^{3+} ion and magnetic ordering at 2.3 K. These results encourage us to pursue the effort of synthesizing bifunctional luminescent molecule-based magnets and extend this approach to different Ln^{3+} ions combined with octacyanomalybdate or octacyanotungstate. The following points justify such an association: (i) The paramagnetic lanthanides have large unquenched orbital moments associated with the internal f magnetic orbitals, giving rise to the high magnetic anisotropy required for the design of magnetically ordered networks with high coercivity. On the other hand, magnetic interactions involving lanthanide ions are weak, and an association of those with transition metal ions should increase the strength of the magnetic interactions, on one hand, and reduce the problem of orbital degeneracy, on the other. For this reason, the association of Ln^{3+} with paramagnetic hexa- and octacyanometalate building blocks seems to be an interesting way to obtain molecule-based magnets. Indeed, numerous one-,[12] two-,[13] and three-dimensional[14] cyano-bridged molecular magnets based on the association of 4f−*n*d (n = 3−5) ions presenting original architectures and interesting magnetic properties have been reported. However, to the best of our knowledge, luminescent properties of these compounds have never been explored, except in the preliminary study of Vogler and Kunkely on a heavy atom effect of $Gd[M(CN)_6]$ (M = Cr, Co) inducing the appearance of phosphorescence under ambient conditions.[15] (ii) The f−f transitions of Ln^{3+} ions are spin- and parity-forbidden,[16] and

(5) (a) Bénard, S.; Pei, Y.; Audiére, J.-P.; Rivière, E.; Clément, R.; Ghilhem, J.; Tchertanov, L.; Nakatani, K. *J. Am. Chem. Soc.* **2000**, *122*, 9444. (b) Bénard, S.; Léaustic, A.; Pei, Y.; Clément, R. *Chem. Mater.* **2001**, *13*, 159. (c) Liu, C.-M.; Zuo, J.-L.; Zhang, D.-Q.; Zhu, D.-B. *CrystalEngComm* **2008**, 1674. (d) Masciocchi, N.; Galli, S.; Sironi, A.; Cariati, E.; Galindo, M. A.; Barea, E.; Romeno, A.; Salas, J. M.; Navarro, J. A. R.; Santoyo-Gonzalez, F. *Inorg. Chem.* **2006**, *45*, 7612–7620.

(6) (a) Maspoch, D.; Domingo, N.; Ruiz-Molina, D.; Wurst, K.; Vaughan, G.; Tejada, J.; Rovira, C.; Veciana, J. *Angew. Chem., Int. Ed.* **2004**, *43*, 1828. (b) Maspoch, D.; Domingo, N.; Ruiz-Molina, D.; Wurst, K.; Tejada, J.; Rovira, C.; Veciana, J. *J. Am. Chem. Soc.* **2004**, *126*, 730. (c) Luo, F.; Che, Y.; Zheng, J. *Crystal Growth&Design.* **2009**, *9*, 1066–1071. (d) Maspoch, D.; Molina, D. R.; Veciana, J. *Chem. Soc. Rev.* **2007**, *36*, 770–818. (e) Kaneko, W.; Ohba, M.; Kitagawa, S. *J. Am. Chem. Soc.* **2007**, *129*, 13706–13712. (f) Yanai, N.; Kaneko, W.; Yoneda, K.; Ohba, M.; Kitagawa, S. *J. Am. Chem. Soc.* **2007**, *129*, 3496–3497.

(7) (a) Coronado, E.; Galàn-Mascaros, J.-R.; Gomez-Garcia, C. J.; Laukhin, V. *Nature* **2000**, *408*, 447. (b) Setifi, F.; Ouahab, L.; Golhen, S.; Yoshida, Y.; Saito, G. *Inorg. Chem.* **2003**, *42*, 1791. (c) Maspoch, D.; Ruiz-Molina, D.; Veciana, J. *Chem. Soc. Rev.* **2007**, *36*, 770–818. (d) Patil, R. M.; Shivkumar, R. *Asian J. of Chemistry* **2008**, *20*, 4477–4484.

(8) For example:(a) Marchal, C.; Filinchuk, Y.; Imbert, D.; Bunzli, J.-C. G.; Mazzanti, M. *Inorg. Chem.* **2007**, *46*, 6242. (b) Liu, W.; Jiao, T.; Li, Y.; Liu, Q.; Tan, M.; Wang, H.; Wang, L. *J. Am. Chem. Soc.* **2004**, *126*, 2280. (c) de Bettencourt-Dias, A. *Inorg. Chem.* **2005**, *44*, 2734. (d) Muller-Buschbaum, K.; Gomez-Torres, S.; Larsen, P.; Wickleder, C. *Chem. Mater.* **2007**, *19*, 655. (e) Mahata, P.; Natarajan, S. *Inorg. Chem.* **2007**, *46*, 1250. (f) Zhao, B.; Chen, X.-Y.; Cheng, P.; Liao, D.-Z.; Yan, S.-P.; Jiang, Z.-H. *J. Am. Chem. Soc.* **2004**, *126*, 15394. (g) Luo, F.; Che, Y.; Zheng, J. *J. Crystal Growth&Design.* **2008**, *8*, 2006–2010. (h) Han, Y.-F.; Zhou, X.-H.; Zheng, Y.-X.; Shen, Z.; Song, Y.; You, X.-Z. *CrystalEngComm.* **2008**, *10*, 1237–1242. (i) Li, X.; Li, Y.-Q.; Zheng, X.-J.; Sun, H.-L. *Inorg. Chem. Commun.* **2008**, *11*, 779–782. (j) Xie, C.; Zhanga, B.; Wanga, X.; Yua, B.; Wanga, R.; Shena, G.; Shena, D. *Z. Anorg. Allg. Chem.* **2008**, *634*, 387–391.

(9) (a) Rueff, J.-M.; Nierengarten, J.-F.; Gilliot, P.; Demessence, A.; Gregut, O.; Drillon, M.; Rabu, P. *Chem. Mater.* **2004**, *16*, 2933. (b) Kahn, O.; Cador, O.; Larionova, J.; Mathonier, C.; Sutter, J.-P. *Mol. Cryst. Liq. Cryst.* **1997**, *305*, 1. (c) Decurtins, S.; Schmalle, H.; Pellaux, R.; Schneuwly, Ph.; Hauser, A. *Inorg. Chem.* **1996**, *35*, 1451.

(10) Chelebaeva, E.; Larionova, J.; Guari, Y.; Ferreira, R. A. S.; Carlos, L. D.; Paz, F. A. A.; Trifonov, A.; Guerin, Ch *Inorganic Chemistry* **2008**, *47*, 775–777.

(11) Harbuzaru, B. V.; Corma, A.; Rey, F.; Atienzar, P.; Jordá, J. L.; García, H.; Ananias, D.; Carlos, L. D.; Rocha, J. *Angew. Chem. Int. Ed.* **2008**, *47*, 1080–1083.

(12) for example(a) Prins, F.; Pasca, E.; de Jongh, L. Jos; Kooijman, H.; Spek, A. L.; Tanase, S. *Angew. Chem. Int. Ed.* **2007**, *46*, 6081. (b) Zhao, H.; Lopez, N.; Prosvirin, A.; Chifotides, H. T.; Dunbar, K. R. *Dalton. Trans.* **2007**, 878. (c) Przychodzen, P.; Lewinski, K.; Pelka, R.; Balanda, M.; Tomala, K.; Sieklucka, B. *Dalton. Trans.* **2006**, 625. (d) Estrader, M.; Ribas, J.; Tangoulis, V.; Solans, X.; Font-Bardia, M.; Maestro, M.; Diaz, C. *Inorg. Chem.* **2006**, *45*, 8239. (e) Ikeda, S.; Hozumi, T.; Hashimoto, K.; Ohkoshi, S.-I *Dalton Trans.* **2005**, *12*, 2120. (f) Tanase, S.; Reedijk, J. *Coord. Chem. Rev.* **2006**, *250*, 2501. (g) Przychodzen, P.; Korzeniak, T.; Podgajny, R.; Sieklucha, B. *Coord. Chem. Rev.* **2006**, *250*, 2234. (h) Figuerola, A.; Diaz, C.; El Fallah, M. S.; Ribas, J.; Maestro, M. *Chem. Commun.* **2001**, 1204. (i) Figuerola, A.; Diaz, C.; Ribas, J.; Tangoulis, V; Sangregorio, C.; Gatteschi, D.; Maestro, M. *Inorg. Chem.* **2003**, *42*, 5274. (j) Gu, Z.-G.; Liu, W.; Yang, Q.-F.; Zhou, X.-H.; Zuo, J.-L.; You, X.-Z. *Inorg. Chem.* **2007**, *46*, 3236–3244. (k) Sereda, O.; Neels, A.; Stoeckli, F.; Stoeckli-Evans, H.; Filinchuk, Y. *Cryst. Growth Des.* **2008**, *8*, 2307–2311. (l) Branzea, D.G.; Guerri, A.; Fabelo, O.; Ruiz-Pérez, C.; Chamoreau, L.-M.; Sangregorio, C.; Caneschi, A.; Andruh, M. *Cryst. Growth Des.* **2008**, *8*, 941–949.

(13) (a) Chen, W.-T.; Guo, G.-C.; Wang, M.-S.; Xu, G.; Cai, L.-Z; Akitsu, T.; Akita-Tanaka, M.; Matsushita, A.; Huang, J.-S. *Inorg. Chem.* **2007**, *46*, 2105. (b) Hozumi, T.; Ohkoshi, S.-I.; Arimoto, Y.; Seino, H.; Mizobe, Y.; Hashimoto, K. *J. Phys. Chem. B* **2003**, *107*, 11571–11574. (c) Kou, H.-Z.; Gao, S.; Jin, X. *Inorg. Chem.* **2001**, *40*, 6295. (d) Ma, B.-Q.; Gao, S.; Su, G; Xu, G.-X. *Angew. Chem. Int. Ed.* **2001**, *40*, 434. (e) Kou, H.-Z.; Gao, S.; Sun, B.-W.; Zhang *J. Chem. Mater.* **2001**, *13*, 1431. (f) Kaneko, S.; Tsunobuchi, Y.; Sakurai, Sh.; Ohkoshi, Sh.-ich. *Chem. Phys. Lett.* **2007**, *446*, 292. (g) Gillon, B.; Goujon, A.; Willemin, S.; Larionova, J.; Desplanches, C.; Ruiz, E.; Stride, J.A.; Guérin, Ch *Inorg. Chem.* **2007**, *46*, 1090–1099.

(14) (a) Hulliger, F.; Landolt, M.; Vetsch, H. *J. Solid State Chem.* **1976**, *18*, 283. (b) Hulliger, F.; Landolt, M.; Vetsch, H. *J. Solid State Chem.* **1976**, *18*, 307. (c) Shiga, T.; Okawa, H.; Kitagawa, S.; Ohba, M. *J. Am. Chem. Soc.* **2006**, *128*, 16426. (d) Chen, Y.; Zhou, H.; Shen, X.; Lu, H.; Yuan, A. *J. of Molecular Structure* **2007**, *839*, 64–68. (e) Podgajny, R.; Pinkowicz, D.; Korzeniak, T.; Nitek, W.; Rams, M.; Sieklucka, B. *Inorg. Chem.* **2007**, *46*, 10416–10425. (f) Milon, J.; Daniel, M.-Ch.; Kaiba, A.; Guionneau, Ph.; Brandes, St.; Sutter, J.-P. *J. Am. Chem. Soc.* **2007**, *129*, 13872–13878. (g) Ohkoshi,, Sh.-ich.; Tsunobuchi, Y.; Takahashi, H.; Hozumi, T.; Shiro, M.; Hashimoto, K. *J. Am. Chem. Soc.* **2007**, *129*, 3084. (h) Podgajny, R.; Chmel, N. P.; Bałanda, M.; Tracz, P.; Gawęl, B.; Zaja, D.; Sikora, M.; Kapusta, C.; Łasocha, W.; Wasiutyn′ski, T.; Sieklucka, B. *J. Mater. Chem.* **2007**, 3308. (i) Ohba, M.; Kaneko, W.; Kitagawa, S.; Maeda, T.; Mito, M. *J. Am. Chem. Soc.* **2008**, *130*, 4475–4484.

(15) Kunkely, H.; Vogler, A. *Inorg. Chem. Commun.* **2004**, *7*, 770.

(16) Bunzli, J.-C. G. *Acc. Chem. Res.* **2006**, *39*, 53.

to exploit the luminescent properties, the two lanthanide transition metal ions as well as the bridging ligand should be carefully chosen in order to prevent the quenching of the Ln^{3+} luminescence by energy transfer processes, namely, high absorption of transition metal ions in the optically active Ln^{3+} spectral regions (the so-called "inner filter" effect). Contrarily to what has been observed in the case of hexacyanoferrate and hexacyanochromates,[17] the $[M(CN)_8]^{3-}$ (M = Mo,W) building blocks do not efficiently absorb Ln^{3+} visible light, not acting, therefore, as dense filters. For this reason, paramagnetic octacyanomalybdate(V) and octacyanotungstate(V) possessing spins equal to 1/2 seem to be interesting building blocks for the design bi-dimensional luminescent magnetic networks in association with Ln^{3+} ions.

In this article, we report the synthesis, structure, and investigations into luminescent and magnetic properties of eight new two-dimensional cyano-bridged coordination polymers $Ln(H_2O)_5[M(CN)_8]$ (where Ln = Eu, Tb, Sm, Gd and M = Mo, W).

Experimental Section

Syntheses. Unless otherwise noted, all manipulations were performed at ambient temperature using reagents and solvents as received. The precursors $(N(C_4H_9)_4)_3[Mo(CN)_8]$[18] and $(N(C_4H_9)_4)_3[W(CN)_8]$[19] were prepared as already described. $[Ln(H_2O)_6](NO_3)_2$ with Ln = Eu and Sm were purchased from ABCR and those with Ln = Tb and Gd from Rhone Poulenc. The acetonitrile and ether used in these experiments were analytical-grade.

$Ln(H_2O)_5[M(CN)_8]$ (Ln = Eu, Tb, Sm, Gd; M = Mo or W). The slow diffusion of a 0.10 M (6 mL) solution of $[(N(C_4H_9)_4]_3[M(CN)_8]\cdot 2H_2O$ and a 0.18 M (3 mL) solution of $[Ln(H_2O)_6](NO_3)_2$ (Ln = Eu, Tb, Gd, Sm) in acetonitrile leads to the formation of highly crystalline compounds after two weeks. The crystals were washed with acetonitrile and dried in the air. The crystals are insoluble in the most common solvents and relatively stable in the air. The composition of the crystalline compound was established by single-crystal X-ray diffraction at 160 K and by elemental analysis.

$Sm(H_2O)_5[Mo(CN)_8]$. Yellow crystals. Elem anal. calcd for $C_8H_{10}N_8O_5SmMo$, %: C, 17.65; Mo, 17.62; N, 20.58; Sm, 27.61. Found: C, 17.20; Mo, 17.06; N, 20.72; Sm, 27.66. IR (KBr): 2128(s), 2161(w), 2157(w), 2173(m) cm^{-1}.

$Eu(H_2O)_5[Mo(CN)_8]$. Yellow crystals. Elem anal. calcd for $C_8H_{10}N_8O_5EuMo$, %: C, 17.59; Eu, 27.83; Mo, 17.57; N, 20.52. Found: C, 17.55; Eu, 27.86; Mo, 17.02; N, 20.45. IR (KBr): 2117(m), 2163(s), 2179(s) cm^{-1}.

$Gd(H_2O)_5[Mo(CN)_8]$. Yellow crystals. Elem anal. calcd for $C_8H_{10}N_8O_5GdMo$, %: C, 17.43; Gd, 28.52; Mo, 17.40; N, 20.32. Found: C, 17.04; Gd, 28.70; Mo, 17.66; N, 20.23. IR (KBr): 2136(s), 2160(s), 2180(s) cm^{-1}.

$Tb(H_2O)_5[Mo(CN)_8]$. Yellow crystals. Elem anal. calcd for $C_8H_{10}N_8O_5TbMo$, %: C, 17.37; Mo, 17.35; N, 20.26; Tb, 28.73. Found: C, 17.01; Mo, 17.58; N, 20.90; Tb, 28.58. IR (KBr): 2133(s), 2161(m), 2177(m) cm^{-1}.

$Sm(H_2O)_5[W(CN)_8]$. Orange crystals. Elem anal. calcd for $C_8H_{10}N_8O_5SmW$, %: C, 15.19; N, 17.72; Sm, 23.78; W, 29.07. Found: C, 15.46; N, 17.13; Sm, 23.35; W, 29.78. IR (KBr): 2133(w), 2163(s), 2178(s) cm^{-1}.

$Eu(H_2O)_5[W(CN)_8]$. Orange crystals. Elem anal. calcd for $C_8H_{10}N_8O_5EuW$, %: C, 15.15; Eu, 23.97; N, 17.67; W, 29.00. Found: C, 15.55; Eu, 23.86, N, 17.45, W, 28.92. IR (KBr): 2117(m), 2163(s), 2179(s) cm^{-1}.

$Gd(H_2O)_5[W(CN)_8]$. Orange crystals. Elem anal. calcd for $C_8H_{10}N_8O_5GdW$, %: C, 15.03; Gd, 24.60; N, 17.53; W, 28.76. Found: C, 15.06; Gd, 24.65; N, 17.09; W, 28.02. IR (KBr): 2135(w), 2164(s), 2180(s) cm^{-1}.

$Tb(H_2O)_5[W(CN)_8]$. Orange crystals. Elem anal. calcd for $C_8H_{10}N_8O_5TbW$, %: C, 14.99; N, 17.48; Tb, 24.79; W, 28.68. Found: C, 14.86; N, 17.23; Tb, 24.88; W, 28.55. IR (KBr): 2133(w), 2164(m), 2181(s) cm^{-1}.

Single-Crystal X-Ray Diffraction. Single crystals of $Ln(H_2O)_5[M(CN)_8]$ (where Ln = Eu, Tb, Sm, Gd and M = Mo, W) were manually harvested from the crystallization vials and mounted on Hampton Research CryoLoops using FOMBLIN Y perfluoropolyether vacuum oil (LVAC 25/6) purchased from Aldrich[20] with the help of a Stemi 2000 stereomicroscope equipped with Carl Zeiss lenses. Data were collected on a Bruker X8 Kappa APEX II charge-coupled device area detector diffractometer (Mo Kα graphite-monochromated radiation, $\lambda = 0.71073$ Å) controlled by the APEX2 software package[21] and equipped with an Oxford Cryosystems Series 700 cryostream monitored remotely using the software interface Cryopad.[22] Images were processed using the software package SAINT+,[23] and data were corrected for absorption using the multiscan semiempirical method implemented in SADABS.[24] Structures were solved using the Patterson synthesis algorithm implemented in SHELXS-97,[25,26] which allowed the immediate location of the Ln^{3+} and M^{5+} metallic centers. All remaining non-hydrogen atoms were located from difference Fourier maps calculated from successive full-matrix least-squares refinement cycles on F^2 using SHELXL-97.[25,27] All non-hydrogen atoms were successfully refined using anisotropic displacement parameters.

The new data sets collected for this system revealed a considerable disorder associated with all cyanide moieties and most of the coordinated water molecules. Indeed, while one coordinated water molecule [O(1W)] retains the same crystallographic position as that previously reported by us for the average model, the second molecule was found to be disordered over three distinct crystallographic positions, O(2W) and O(3W) (Figure 1a), with fixed rates of occupancy of 40%/30%/30% (calculated from unrestrained model refinement). All cyanide ligands were found to be equally disordered over two distinct crystallographic positions (Figure 1b). Even though the hydrogen atoms associated with the coordinated water molecules couldn't be located from difference Fourier maps and attempts to include these in calculated positions didn't lead to sensible structural refinements, they have been included in the empirical formulae of the materials (Table 1).

The last difference Fourier map syntheses showed, respectively, the highest peak and deepest hole (see Table 1 for individual data) located at, for $Eu(H_2O)_5[Mo(CN)_8]$, 0.76 Å from O(3W) and 2.27 Å from N(2); for $Gd(H_2O)_5[Mo(CN)_8]$, 0.61 Å and 0.12 Å from Gd(1); for $Tb(H_2O)_5[Mo(CN)_8]$, 0.90 Å from

(17) The compounds $Tb[Fe(CN)_6]$ and $Eu[Fe(CN)_6]$ don't present the luminescence in the visible region.

(18) Mascharah, P. K. *Inorg. Chem.* **1986**, *25*, 15.
(19) Leipold, J.G.; Bok, L.D.C. *Z. Anorg. Allg. Chem.* **1974**, *407*, 350–352.
(20) Kottke, T.; Stalke, D. *J. App. Cryst.* **1993**, *26*, 615–619.
(21) APEX2, *Data Collection Software Version 2.1-RC13*, Bruker AXS, Delft, The Netherlands 2006.
(22) Cryopad, *Remote monitoring and control, Version 1.451, Oxford Cryosystems*, Oxford, United Kingdom 2006.
(23) SAINT+, *Data Integration Engine v. 7.23a* © 1997-2005, Bruker AXS, Madison, Wisconsin, USA.
(24) Sheldrick, G. M., *SADABS v.2.01, Bruker/Siemens Area Detector Absorption Correction Program* 1998, Bruker AXS, Madison, Wisconsin, USA.
(25) Sheldrick, G. M. *Acta Cryst. A* **2008**, *64*, 112–122.
(26) Sheldrick, G. M., *SHELXS-97, Program for Crystal Structure Solution*, University of Göttingen 1997.
(27) Sheldrick, G. M., *SHELXL-97, Program for Crystal Structure Refinement*, University of Göttingen 1997.

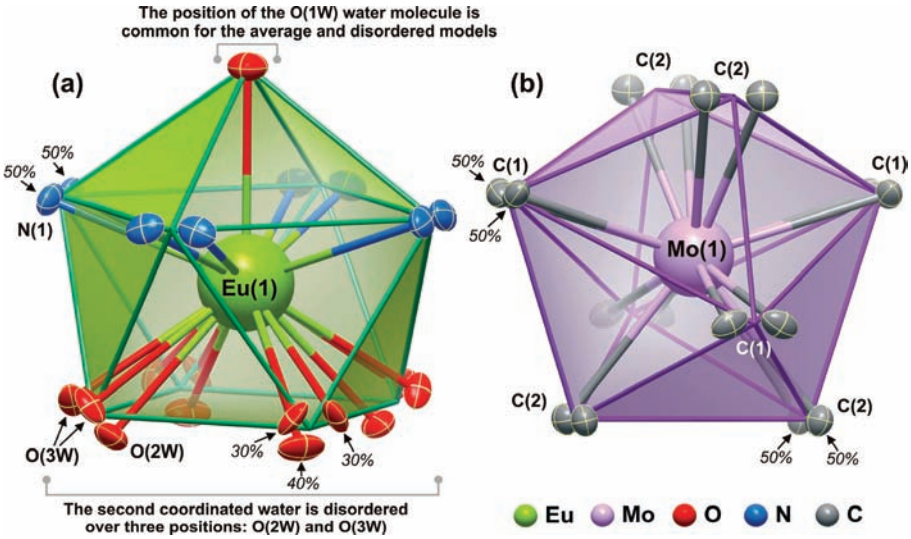

Figure 1. Schematic representation of the average (a) tricapped trigonal prismatic $\{LnN_4O_5\}$ and (b) dodecahedral $\{MoC_8\}$ coordination environments of the metallic centers composing the crystal structure of $Eu(H_2O)_5[Mo(CN)_8]$. The labelling scheme and the rates of occupancy for all atoms composing the first coordination spheres are also given. Atoms from the ligands are represented as thermal ellipsoids drawn at the 30% probability level. Symmetry operations used to generate equivalent atoms have been omitted for clarity purposes.

Tb(1) and 0.95 Å from O(1W); for $Sm(H_2O)_5[W(CN)_8]$, 1.17 Å and 1.55 Å from O(1W); for $Eu(H_2O)_5[W(CN)_8]$, 0.83 Å from Eu(1) and exactly at the W(1) position; for $Gd(H_2O)_5[W(CN)_8]$, 1.17 Å and 0.69 Å from Gd(1); and for $Tb(H_2O)_5[W(CN)_8]$, 0.65 Å from Tb(1) and 1.43 Å from O(1W).

Information concerning crystallographic data collection and structure refinement details for the eight structures is summarized in Table 1. Selected bond lengths for the $\{LnN_4O_5\}$ and $\{MC_8\}$ coordination environments are collected in Table 2.

Powder X-Ray Diffraction. Conventional powder X-ray diffraction data were collected at ambient temperature on an X'Pert MPD Philips diffractometer (Cu $K\alpha_{1,2}$ X-radiation, $\lambda_1 = 1.540598$ Å and $\lambda_2 = 1.544426$ Å), equipped with a flat-plate sample holder in a Bragg−Brentano para-focusing optics configuration (40 kV, 50 mA). Intensity data were collected using the step-counting method (step 0.033°), in continuous mode, in the $5 \leq 2\theta \leq 90°$ range.

The experimental powder X-ray diffraction pattern of $Sm(H_2O)_5[Mo(CN)_8]$ was indexed using DICVOL04[28] from the first 20 and most intense resolved reflections [absolute error 0.03° 2θ; M(20)[29] = 62.1; F(20)[30] = 73.0; zero shift 2θ = 0.0°], thus confirming the general structural homologies with the remaining members of the series. A Le Bail[31] whole-powder-diffraction-pattern profile fitting (not shown) in the tetragonal *P4/nmm* space group (identified using CHECKCELL)[32] was performed with the FullProf.2k software package.[33,34] The final profile fitting (R_{Bragg} = 9.61% and χ^2 = 3.99) was obtained using a typical pseudo-Voigt peak-shape function. Fixed (manually selected) background points were employed. The unit cell parameters of $Sm(H_2O)_5[Mo(CN)_8]$ converged to a = 10.9190(9) Å and c = 7.2855(7) Å.

Physical Measurements. Infrared spectra were recorded as KBr disks or Nujol mulls between NaCl plates on a Nicolet Model 510P spectrophotometer. Thermogravimetry analyses were performed using a Netzsch STA 409 instrument under an argon atmosphere from 30 to 700 °C at a heating rate of 1 °C min^{-1}. Elemental analyses were performed by the Service Central d'Analyses (CNRS, Vernaison, France). The samples were heated at 3000 °C under He. Oxygen was transformed in CO and detected by using an IR detector. Metals were determined with a high-resolution inductively coupled plasma mass spectrometer using a ThermoFischer element. The photoluminescence spectra were recorded between 14 K and room temperature on a Fluorolog-3 model FL3-2T with double excitation spectrometer and a single-emission spectrometer (TRIAX 320) coupled to an R928 photomultiplier, using a front face acquisition mode. The excitation source was a 450 W xenon lamp. Emission was corrected for the spectral response of the monochromators and the detector using a typical correction spectrum provided by the manufacturer, and the excitation spectra were corrected for the spectral distribution of the lamp intensity using a photodiode reference detector. The lifetime measurements were acquired between 14 K and room temperature with the setup described for the luminescence spectra using a pulsed Xe−Hg lamp (6 μs pulse at half width and 20−30 μs tail). Magnetic susceptibility data were collected with a Quantum Design MPMS-XL SQUID magnetometer working in the temperature range 1.8−350 K and up to 5 T. The crystals have been triturated before being placed in the sample holder. The magnetic measurements of all samples have been performed with the fast cooling of the samples to 10 K. Data were corrected for the sample holder and the diamagnetism contributions calculated from the Pascal's constants.[35]

Results and Discussion

Synthesis and Crystal Structure. The slow diffusion of ether into a 2×10^{-4} M solution of $[(N(C_4H_9)_4]_3[M(CN)_8]\cdot 2H_2O$ (M = Mo or W) and $[Ln(H_2O)_n](NO_3)_2$ (Ln = Eu,

(28) Boultif, A.; Louer, D. *J. App. Cryst.* **2004**, *37*, 724–731.
(29) Boultif, A.; Louer, D. *J. App. Cryst.* **1991**, *24*, 987–993.
(30) Louer, D., In *Automatic Indexing: Procedures and Applications, Accuracy in Powder Diffraction II*, Gaithersburg, MD, USA, 1992; pp. 92-104.
(31) LeBail, A.; Duroy, H.; Fourquet, J. L. *Mater. Res. Bull.* **1988**, *23*(3), 447–452.
(32) Laugier, J.; Bochu, B., *CHECKCELL - A Software Performing Automatic Cell/Space Group Determination, Collaborative Computational Project Number 14 (CCP14), Laboratoire des Matériaux et du Génie Physique de l'Ecole Supérieure de Physique de Grenoble (INPG), France*, **2000**.
(33) Rodriguez-Carvajal, J., *FULLPROF - A Program for Rietveld Refinement and Pattern Matching Analysis, Abstract of the Satellite Meeting on Powder Diffraction of the XV Congress of the IUCR*, Toulouse, France, 1990, p.127.
(34) Roisnel, T.; Rodriguez-Carvajal, J., *WinPLOTR [June 2005] - A Windows Tool for Powder Diffraction Pattern Analysis. Materials Science Forum, Proceedings of the Seventh European Powder Diffraction Conference (EPDIC 7)*, **2000**, p.118-123, Ed. R. Delhez and E.J. Mittenmeijer.
(35) *Theory and Applications of Molecular Paramagnetism*, Eds. Boudreaux, E. A. L.; Mulay, N. John Wiley Sons, New York, 1976.

Table 1. Crystal and Structure Refinement Data for $Ln(H_2O)_5[M(CN)_8]$ (where Ln = Eu, Gd, Tb and Sm and M = Mo or W)

	$Eu(H_2O)_5$-$[Mo(CN)_8]$	$Gd(H_2O)_5$-$[Mo(CN)_8]$	$Tb(H_2O)_5$-$[Mo(CN)_8]$	$Sm(H_2O)_5$-$[W(CN)_8]$	$Eu(H_2O)_5$-$[W(CN)_8]$	$Gd(H_2O)_5$-$[W(CN)_8]$	$Tb(H_2O)_5$-$[W(CN)_8]$
formula	$C_8H_{10}EuMoN_8O_5$	$C_8H_{10}GdMoN_8O_5$	$C_8H_{10}MoN_8O_5Tb$	$C_8H_{10}N_8O_5SmW$	$C_8H_{10}EuN_8O_5W$	$C_8H_{10}GdN_8O_5W$	$C_8H_{10}N_8O_5TbW$
fw	546.14	551.43	553.10	632.44	634.05	639.34	641.01
cryst syst	tetragonal	tetragonal	tetragonal	tetragonal	tetragonal	tetragonal	tetragonal
space group	*P*4/*nmm*	*P*4/*nmm*	*P*4/*nmm*	*P*4/*nmm*	*P*4/*nmm*	*P*4/*nmm*	*P*4/*nmm*
temp/K	180(2)	180(2)	180(2)	200(2)	150(2)	150(2)	150(2)
a,*b*/Å	10.9601(4)	10.9175(2)	10.8912(2)	10.9749(4)	10.9793(6)	10.9500(16)	10.9183(12)
c/Å	7.1282(4)	7.1541(2)	7.1961(2)	7.1697(7)	7.1119(9)	7.167(3)	7.1633(19)
volume/Å^3	856.27(7)	852.71(3)	853.59(3)	863.58(10)	857.30(13)	859.4(4)	853.9(3)
Z	2	2	2	2	2	2	2
D_{calcd}/g cm^{-3}	2.118	2.148	2.152	2.432	2.456	2.471	2.493
μ(Mo Kα)/mm^{-1}	4.395	4.625	4.878	10.055	10.362	10.546	10.871
cryst size/mm	0.20×0.14×0.10	0.55×0.30×0.30	0.18×0.10×0.08	0.16×0.10×0.06	0.16×0.10×0.06	0.16×0.16×0.10	0.26×0.20×0.18
crystal type	yellow blocks	yellow blocks	yellow blocks	yellow blocks	yellow blocks	yellow blocks	yellow blocks
θ range	3.72−29.12	3.73−43.89	3.74−31.49	3.71−50.03	3.71−40.25	3.72−29.02	3.73−40.24
index ranges	$-14 \le h \le 14$ $-11 \le k \le 14$ $-8 \le l \le 9$	$-14 \le h \le 20$ $-20 \le k \le 19$ $-13 \le l \le 13$	$-15 \le h \le 15$ $-14 \le k \le 15$ $-10 \le l \le 10$	$-23 \le h \le 23$ $-23 \le k \le 22$ $-15 \le l \le 13$	$-19 \le h \le 15$ $-18 \le k \le 19$ $-12 \le l \le 12$	$-14 \le h \le 12$ $-14 \le k \le 10$ $-9 \le l \le 9$	$-15 \le h \le 19$ $-19 \le k \le 17$ $-12 \le l \le 12$
reflns collected	16702	33477	16428	47825	23795	6452	22792
independent reflns	674 (R_{int} = 0.0308)	1830 (R_{int} = 0.0299)	825 (R_{int} = 0.0321)	2496 (R_{int} = 0.0273)	1486 (R_{int} = 0.0637)	647 (R_{int} = 0.0633)	1494 (R_{int} = 0.0665)
data completeness	up to θ = 29.12°, 99.4%	up to θ = 43.89°, 98.3%	up to θ = 31.49°, 99.4%	up to θ = 50.03°, 98.6%	up to θ = 40.25°, 97.3%	up to θ = 29.02°, 95.3%	up to θ = 40.24°, 98.3%
final R indices $[I > 2\sigma(I)]^{a,b}$	R1 = 0.0149 wR2 = 0.0430	R1 = 0.0179 wR2 = 0.0494	R1 = 0.0143 wR2 = 0.0386	R1 = 0.0156 wR2 = 0.0343	R1 = 0.0217 wR2 = 0.0409	R1 = 0.0286 wR2 = 0.0801	R1 = 0.0224 wR2 = 0.0548
final R indices (all data)^{a,b}	R1 = 0.0152 wR2 = 0.0432	R1 = 0.0190 wR2 = 0.0500	R1 = 0.0153 wR2 = 0.0392	R1 = 0.0172 wR2 = 0.0349	R1 = 0.0264 wR2 = 0.0419	R1 = 0.0337 wR2 = 0.0950	R1 = 0.0243 wR2 = 0.0558
weighting scheme^c	*m* = 0.0262 *n* = 0.6530	*m* = 0.0315 *n* = 0.2280	*m* = 0.0213 *n* = 0.7022	*m* = 0.0148 *n* = 0.4451	*m* = 0.0124 *n* = 0.8675	*m* = 0.0532 *n* = 0.2929	*m* = 0.0180 *n* = 2.3026
largest diff. peak and hole	0.453 and −1.473 eÅ^{-3}	1.625 and −2.219 eÅ^{-3}	0.937 and −0.561 eÅ^{-3}	3.480 and −2.934 eÅ^{-3}	1.258 and −4.264 eÅ^{-3}	1.761 and −3.697 eÅ^{-3}	1.404 and −5.471 eÅ^{-3}
CCDC number	682457	683679	683680	682458	682459	682460	682461

^{a} $R1 = \sum ||F_o| - |F_c||/\sum |F_o|$. ^{b} $wR2 = \sqrt{\sum[w(F_o^2 - F_c^2)^2]/\sum[w(F_o^2)^2]}$. ^{c} $w = 1/[\sigma^2(F_0^2) + (mP)^2 + nP]$ where $P = (F_o^2 + 2F_c^2)/3$.

Table 2. Selected Bond Lengths (in Å) for the $\{LnN_4O_5\}$ and $\{MC_8\}$ Coordination Environments Present in $Ln(H_2O)_5[M(CN)_8]$ (where Ln = Sm, Eu, Gd or Tb, and M = Mo or W)

	$Eu(H_2O)_5[Mo(CN)_8]$	$Gd(H_2O)_5[Mo(CN)_8]$	$Tb(H_2O)_5[Mo(CN)_8]$
Ln(1)−O(1W)	2.526(4)	2.525(3)	2.521(4)
Ln(1)−O(2W)	2.423(8)	2.407(5)	2.384(8)
Ln(1)−O(3W)	2.479(6)	2.459(3)	2.469(6)
Ln(1)−N(1)	2.523(3)	2.5020(18)	2.490(3)
M(1)−C(1)	2.157(4)	2.1470(18)	2.150(3)
M(1)−C(2)	2.148(3)	2.1462(18)	2.149(3)

	$Sm(H_2O)_5[W(CN)_8]$	$Eu(H_2O)_5[W(CN)_8]$	$Gd(H_2O)_5[W(CN)_8]$	$Tb(H_2O)_5[W(CN)_8]$
Ln(1)−O(1W)	2.547(3)	2.525(4)	2.559(14)	2.523(6)
Ln(1)−O(2W)	2.430(6)	2.420(7)	2.439(15)	2.377(9)
Ln(1)−O(3W)	2.485(4)	2.475(5)	2.451(11)	2.465(7)
Ln(1)−N(1)	2.5356(18)	2.528(3)	2.516(9)	2.497(4)
M(1)−C(1)	2.1534(18)	2.154(3)	2.150(10)	2.152(4)
M(1)−C(2)	2.1509(18)	2.156(3)	2.164(10)	2.155(4)

Tb, Sm, Gd) in acetonitrile leads to the formation of yellow (Mo-containing compounds) or orange (W-containing compounds) single crystals. All compounds have been fully characterized by elemental analysis, FT-IR spectroscopy, and single-crystal X-ray crystallography (Table 1). FT-IR C−N stretches for all compounds are shifted toward higher frequencies from those of $[(N(C_4H_9)_4]_3[Mo(CN)_8]$ (2179 (w), 2136 (s) cm^{-1}) and $[(N(C_4H_9)_4]_3[W(CN)_8]$ (2181 (s), 2137 (s) cm^{-1}), showing a coordination of the CN groups to Ln^{3+}.[35] The presence of ν(C−N) in the range 2120−2130 cm^{-1} suggests the existence of terminal cyano groups.

Single-crystal X-ray diffraction studies at low temperatures between 150 and 200 K reveal the presence of isostructural materials, ultimately formulated as $Ln(H_2O)_5[M(CN)_8]$ (Ln = Eu, Tb, Sm, Gd; M = Mo, W). Interestingly, the $Sm(H_2O)_5[Mo(CN)_8]$ material could not be isolated as single crystals of sufficient quality for analysis. Instead, a Le Bail fitting with conventional powder X-ray diffraction data clearly supports the presence of an identical material (not shown). All compounds crystallize in the tetragonal crystal system with overall *P*4/*nmm* space group symmetry (Table 1). For clarity, we shall focus only on the

geometrical details of the $Eu(H_2O)_5[Mo(CN)_8]$ structure in the following paragraphs. Table 2 collects the Ln−(O, N) and M−C bond distances for all structures.

The asymmetric units are composed by two crystallographically independent metallic centers, M(1) and Ln(1), both located at special crystallographic positions. It is important to emphasize that a considerable amount of statistical structural disorder was found for the first coordination spheres of both metallic centers (details on the structural modeling are given in the dedicated Experimental Section). Indeed, all positions are, at least, split into two, giving rise to a distribution of possible coordination spheres, as represented in Figure 1. Nevertheless, M(1) appears in the structures coordinated to eight cyanides, with the overall $\{MC_8\}$ coordination geometry resembling a slightly distorted dodecahedron (Figure 1). Such coordination geometry is characteristic for one-, two-, and three-dimensional coordination polymers containing $[M(CN)_8]^{4-}$ units where M = Mo or W.[36] The single Mo−C bond lengths are 2.157(4) and 2.148(3) Å (Table 2), which is in the range of the bond lengths previously observed for the $[M(CN)_8]^{4-}$ containing coordination polymers.[36] The coordination sphere of the Ln^{3+} centers is composed of four bridging cyanide groups plus five water molecules, $\{LnN_4O_5\}$, overall describing a slightly distorted tricapped trigonal prismatic coordination environment with the Ln−(N,O) bond lengths ranging from 2.423(8) to 2.526(4) Å.

Intermetallic connectivity is achieved via the μ_2-cyanide bridges, ultimately leading to the formation of neutral two-dimensional $_\infty^2[Ln(H_2O)_5M(CN)_8]$ corrugated layers placed in the *ab* crystallographic plane. As also represented in Figure 2, the considerable structural disorder associated with the local coordination environments has little influence on the overall features of the layer. The Eu(1)···Mo(1) intermetallic distance is 5.7803(2) Å for $Eu(H_2O)_5[Mo(CN)_8]$. Despite the structural disorder, the cyanide ligands have low steric hindrance, which leads to a considerable proximity between corrugated layers close-packing along the [001] crystallographic direction (Figure 2b). Indeed, for all structures, the shortest Ln(1)···Ln(1) and Mo (1)···Mo(1) intermetallic distances are those occurring across layers (i.e., the length of the *c* axis for each compound, see Table 1). Connections between layers are assured by very strong O−H···N hydrogen bonds linking the coordinated molecules from one layer to the unidentate (and disordered) C−N cyanide groups from the layer which is immediately adjacent (not shown).

Photoluminescence Measurements. The quantum efficiency of an f−f transition is determined by the ratio between the radiative and nonradiative transition probabilities.[37a] The latter term depends on the energy gap between the emitting level and the level lying just below and on the host vibrations' maximum frequency.[37b] When the energy gap is small (e.g. Sm^{3+} and Dy^{3+}, 7500 cm^{-1}), it could be efficiently bridged by nonradiative processes involving the host lattice vibrational states, and then low quantum efficiencies are, in principle, expected. On the contrary, higher quantum efficiencies are usually observed for ions with large energy gaps (e.g., Gd^{3+}, Tb^{3+}, and Eu^{3+} = 12 000, 15 000, and 33 000 cm^{-1}, respectively).[37b] This is indeed one of the reasons justifying the extensive use of Eu^{3+} and Tb^{3+} ions. However and despite its large energy gap, the photoluminescence features of Gd^{3+}-containing materials are scarcely reported as Gd^{3+} absorption and emission lies in the UV region, superimposing in many cases the absorption/emission of the ligands. Moreover, as in $Sm(H_2O)_5[M(CN)_8]$ (M = Mo, W) crystals, the intra-$4f^5$ lines are not detected (14−300 K), pointing out a high nonradiative transition probability; we will focus the photoluminescence discussion on $Ln(H_2O)_5[M(CN)_8]$ (Ln = Eu, Tb and M = Mo, W).

Figure 3A shows the 14 K excitation spectra of the $Eu(H_2O)_5[W(CN)_8]$ and $Tb(H_2O)_5[W(CN)_8]$ complexes monitored within the $^5D_0 \rightarrow {}^7F_2$ and $^5D_4 \rightarrow {}^7F_5$ transitions, respectively. The spectra display a large broad band with a structured profile in the UV spectral region. For the $Eu(H_2O)_5[W(CN)_8]$ crystals, a series of intra-$4f^6$ lines ascribed to transitions between the $^7F_0$ states and the $^5D_{4,2,1}$, $^5G_{2\text{-}4}$, and $^5L_6$ excited levels is also observed. The higher relative intensity of the intra-$4f^6$ lines relative to that of the broad band indicates that direct intra-$4f^6$ excitation is the more efficient path to sensitizing the Eu^{3+} excited states, contrary to that found for the $Tb(H_2O)_5[W(CN)_8]$ crystal where the main excitation path is via the large broad band. Figure 3 also shows the excitation spectra of the $Eu(H_2O)_5[Mo(CN)_8]$ monitored under the same experimental conditions as those of the W-based crystals. Similarly to that found for the $Eu(H_2O)_5[W(CN)_8]$ crystals, the spectrum of the $Eu(H_2O)_5[Mo(CN)_8]$ crystal is dominated by the Eu^{3+} intra-$4f^6$ lines, a lower-relative intensity band in the UV region also being detected, which will be discussed in detail next.

Comparing the previous spectra with that recently reported for the analogous $Tb(H_2O)_5[Mo(CN)_8]$ (also shown in Figure 3),[10] it is observed that, in the presence of W^{5+}, the spectra are dominated by the $^7F_6 \rightarrow {}^5G_{4\text{-}6}$, $^5L_{10}$, and $^5D_{0,1,3}$ intra-$4f^8$ transitions, indicating that the replacement of Mo^{5+} by W^{5+} ions contributes to a better shielding of the Tb^{3+} ions and to the appearance of another excitation path in the UV spectral region. The large broad bands detected in the UV regions of all of the crystals have also been observed in other materials containing W^{5+} or Mo^{5+} ions, being attributed to the presence of ligand-to-metal charge-transfer (LMCT) transitions resulting from the interaction between the lanthanide (Eu^{3+}, Tb^{3+}) ions and the ligands, namely, LMCT states associated with O → Eu/Tb, O → W, and

(36) (a) Larionova, J.; Willemin, S.; Donnadieu, B.; Henner, B.; Guerin, Ch.; Gillon, B.; Goujon, A. *J. Phys. Chem. Sol* **2004**, *65*, 677–691. (b) Rombaut, G.; Verelst, M.; Golhen, S.; Ouahab, L.; Mathonière, C.; Kahn, O. *Inorg. Chem.* **2001**, *40*, 1151–1159. (c) Rombaut, G.; Golhen, S.; Ouahab, L.; Mathonière, C.; Kahn, O. *J. Chem. Soc., Dalton. Trans.* **2000**, 3609–3614. (d) Rombaut, G.; Mathonière, C.; Guionneau, Ph.; Golhen, S.; Ouahab, L.; Verelst, M.; Lecante, P. *Inorg. Chimica Acta* **2001**, *326*, 27–36. (e) Sra, A. K.; Andruh, M.; Kahn, O.; Golhen, S.; Ouahab, L.; Yakhmi, J. V. *Angew. Chem. Int. Ed. Engl.* **1999**, *38*, 2606–2609. (f) Lu, J.; Harrison, W. T. A.; Jacobson, A. J. *Angew. Chem. Int. Ed. Engl.* **1995**, *34*, 2557–2559.

(37) (a) Carlos, L. D.; Ferreira, R. A. S.; de Zea Bermudez, V.; Ribeiro, S. J. L. *Adv. Mater.* **2009**, *21*, 509–534. (b) Blasse G, Grabmaier B. C., *Luminescent Materials*, Springer-Verlag, Berlin, 1994.

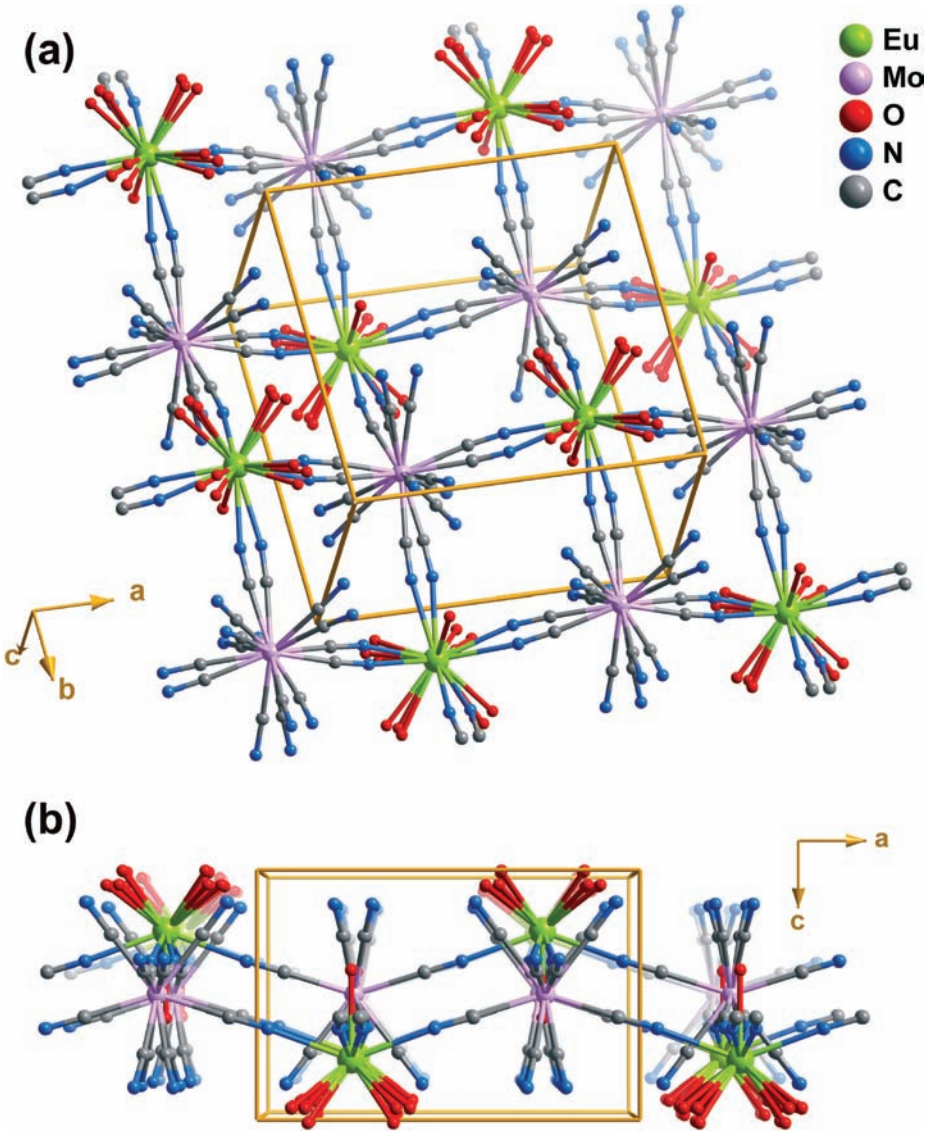

Figure 2. Perspective views of the neutral two-dimensional $_{\infty}^{2}$[$Eu(H_2O)_5Mo(CN)_8$] corrugated layers composing the crystal structure of $Eu(H_2O)_5[Mo(CN)_8]$, showing the structural disorder associated with all cyanide groups and the coordinated water molecules.

O → Mo transitions.[38−44] In the case of the Tb^{3+}-containing crystals, the spin-forbidden (low-spin, LS, and high-spin, HS) interconfigurational fd transitions are discerned around 240 and 280 nm, respectively.[45] The reports found in the literature place the O → W LMCT in a broad wavelength interval from 195 to 325 nm. For instance, lower-energy LMCT states were reported for the polyoxometalate (POM) $K_{13}Eu(SiW_{11}O_{39})$,[40] whereas those at higher wavelengths were found for the $Na_9Eu_{10}O_{36}$ POM[42] and in Eu^{3+}/Tb^{3+} mixed polyoxometallolanthanoates.[41] The O → Mo LMCT states are known to be red-shifted relative to those of O → W being observed, for example, within 290−410 nm for $Eu_2(H_2O)_{12}[Mo_8O_{27}]\cdot 6H_2O$ and around 350 nm for $NaM(WO_4)(MoO_4)$.[39,46] LMCT states ascribed to O → Eu have small extinction coefficients and are expected to lie within 240−250 nm.[44]

In order to get further knowledge on the origin of the broad bands in the present work, Figure 3B shows a detailed comparison of these excitation components in the four crystals. For the $Tb(H_2O)_5[W(CN)_8]$ crystals, two main components are discerned around 257 and 280 nm, whereas for $Eu(H_2O)_5[W(CN)_8]$, two components at 270 and 292 nm and a shoulder at 257 nm are clearly distinguishable. For $Eu(H_2O)_5[Mo(CN)_8]$, the broad band displays components at 250, 270, and 292 nm. Because the band at 257 nm is common to the Eu^{3+}- and Tb^{3+}-based crystals containing W^{5+} ions, it

(38) Naruke, H.; Yamase, T. *J. of Luminescence* **1991**, *50*(1), 55–60.
(39) Yamase, T.; Naruke, H. *J. Chem. Soc.-Dalton Trans.* **1991**, *2*, 285–292.
(40) Wang, J.; Wang, H. S.; Fu, L. S.; Liu, F. Y.; Zhang, H. J. *Thin Solid Films* **2002**, *414*(2), 256–261.
(41) Yamase, T.; Naruke, H. *J. of Physical Chemistry B* **1999**, *103*(42), 8850–8857.
(42) Blasse, G.; Dirksen, G. J.; Zonnevijlle, F. *J. of Inorganic & Nuclear Chemistry* **1981**, *43*(11), 2847–2853.
(43) Ballardini, R.; Mulazzani, Q. G.; Venturi, M.; Bolletta, F.; Balzani, V. *Inorganic Chemistry* **1984**, *23*(3), 300–305.
(44) Ballardini, R.; Chiorboli, E.; Balzani, V. *Inorganica Chimica Acta-F-Block Elements Articles and Letters* **1984**, *95*(6), 323–327.
(45) Pierterson, L.; Reid, M .F.; Burdick, G. W.; Meijerink, A. *Phys. Rev. B* **2002**, *65*, 045114/1–045114/13.
(46) Neeraj, S.; Kijima, N.; Cheetham, A. K. *Chemical Physics Letters* **2004**, *387*(1-3), 2–6.

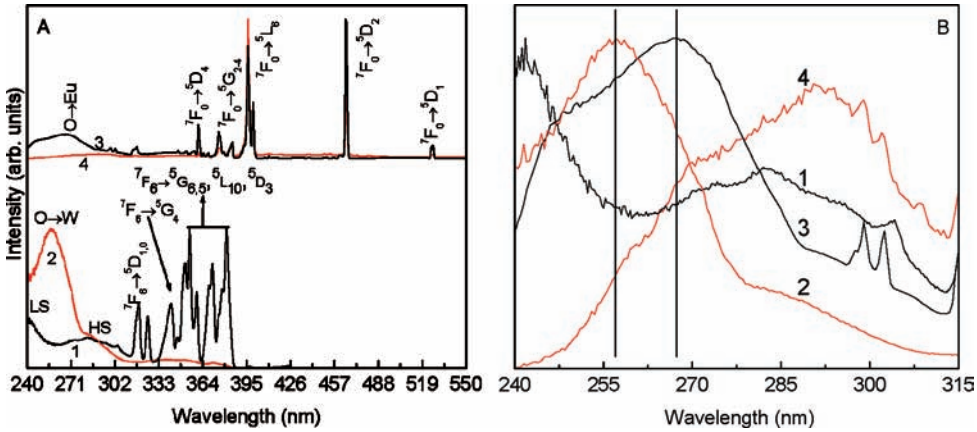

Figure 3. (A) Excitation spectra acquired at 14 K for the (1) $Tb(H_2O)_5[Mo(CN)_8]$,[10] (2) $Tb(H_2O)_5[W(CN)_8]$, (3) $Eu(H_2O)_5[Mo(CN)_8]$, and (4) $Eu(H_2O)_5[W(CN)_8]$ crystals monitored at 618 ($^5D_0 \rightarrow {}^7F_2$) and 544 nm ($^5D_4 \rightarrow {}^7F_5$). (B) Magnification of the 240−315 nm region.

may be readily assigned to the O → W LMCT transition. The excitation component at 270 nm detected in the spectra of Eu-containing crystals may be attributed to O → Eu LMCT states. The O → Mo LMCT states cannot be unequivocally assigned due to the large superposition of excitation components in the 270−310 nm spectral range, arising probably from the large structural disorder typical of these crystals.

The effect of the temperature on the lanthanide ions' excitation paths was studied through the measurement of the room temperature excitation spectra (not shown). For the Eu^{3+}-containing crystals, the increase in temperature up to 300 K induces a decrease in the relative intensity of the broad LMCT bands with respect to the intensity of the intra-$4f^6$ lines, indicating that the energy conversion of the LMCT states to the Eu^{3+}-emitting levels may be thermally deactivated, which is a typical behavior of the LMCT bands.[47] The excitation spectra of $Tb(H_2O)_5[W(CN)_8]$ resemble that previously reported for analogous $Tb(H_2O)_5[Mo(CN)_8]$,[10] showing the Tb^{3+} intra $4f^8$ transitions ($^7F_6 \rightarrow {}^5G_{4\text{-}6}$, $^5L_{10}$, $^5D_{0,1,3}$) and the low-intensity band in the UV region.

Figure 4 compares the 14 K emission spectra of the $Eu(H_2O)_5[Mo(CN)_8]$ crystals under direct intra-$4f^6$ excitation ($^5L_6$, 395 nm). All spectra are formed of the Eu^{3+} intra-$4f^6$ lines attributed to the $^5D_0 \rightarrow {}^7F_{0-4}$ transitions, being observed one, three, and five components for the $^5D_0 \rightarrow {}^7F_{0-2}$ transitions, respectively (Figure 4B−D). Moreover, the higher intensity of the $^5D_0 \rightarrow {}^7F_2$ transition points out that the Eu^{3+} local group is characterized by low site symmetry without an inversion center, in good agreement with the crystallographic studies. Indeed, the presence of a single line for the non-degenerated $^5D_0 \rightarrow {}^7F_0$ transition is in good agreement with the fact that all of the Eu^{3+} ions occupy the same average local environment within each crystal. In order to get further insight into the Eu^{3+} local coordination, the energy, E_{00}, and the full-width-at-half-maximum, $fwhm_{00}$, of the non-degenerated $^5D_0 \rightarrow {}^7F_0$ transition were estimated. The same E_{00} value, 17 226.4 ± 0.2 cm^{-1}, was found for the Mo- and W-containing crystals, pointing out the same Eu^{3+} coordination sphere in both crystals. The high $fwhm_{00}$ values, namely, 31.8 ± 1.0 and 22.6 ± 0.4 cm^{-1} for $Eu(H_2O)_5[W(CN)_8]$ and $Eu(H_2O)_5[Mo(CN)_8]$, respectively, are compatible with a broad distribution of Eu^{3+} local environments, as pointed out by the X-ray diffraction studies.

The Tb^{3+} intra-$4f^8$ $^5D_4 \rightarrow {}^7F_{6\text{-}2}$ transitions, monitored at 14 K, for $Tb(H_2O)_5[W(CN)_8]$, are shown in Figure 5. Varying the excitation wavelength induces minor changes in the relative intensity and in the fwhm, as illustrated for the $^5D_4 \rightarrow {}^7F_5$ transition (inset in Figure 5). Those fwhm values reflect a broad distribution of closely equivalent Tb^{3+} local environments, as in analogous Eu^{3+}-based compounds.

For all crystals, besides an intensity decrease, the room-temperature emission features resemble those acquired at 14 K (Figures 4 and 5).

The Eu^{3+} $^5D_0$ and the Tb^{3+} $^5D_4$ lifetime (τ_{exp}) values were estimated through the monitoring of the respective emission curves around 618 and 544 nm, respectively (corresponding excitation wavelengths of 395 and 355 nm, repectively). All decay curves are well reproduced by a single exponential function. For $Eu(H_2O)_5[W(CN)_8]$ and $Eu(H_2O)_5[Mo(CN)_8]$, the $^5D_0$ lifetime values are 0.948 ± 0.010 ms and 1.107 ± 0.004 ms, respectively, whereas for $Tb(H_2O)_5[W(CN)_8]$, a $^5D_4$ lifetime value of 0.314 ± 0.02 ms was estimated. The value reported for the $Tb(H_2O)_5[Mo(CN)_8]$ analog is 1.313 ± 0.014 ms (excitation wavelength of 380 nm).[10] Under direct intra-4f excitation, the $^5D_0$ and $^5D_4$ lifetime values of the W^{5+}-containing crystals are smaller than those containing Mo^{5+}, which may indicate a higher nonradiative transition probability for the materials with W^{5+}. As the radiative transition probability, A_r (calculated from the relative intensities of the $^5D_0 \rightarrow {}^7F_{0\text{-}4}$ transitions with the $^5D_0 \rightarrow {}^7F_1$ transition as a reference for the whole spectrum[48]), is approximately the same for the $Eu(H_2O)_5[W(CN)_8]$ and $Eu(H_2O)_5[Mo(CN)_8]$ crystals, the differences in the lifetime ($\tau_{exp}^{-1} = A_r + A_{nr}$) between the two types of crystals should be associated with the nonradiative transition probability, A_{nr}.

Magnetic Properties. The difficulty in studying the magnetic properties of compounds containing paramagnetic Ln^{3+} ions arises from the fact that these ions

(47) de Sa, G. F.; Malta, O. L.; Donega, C. D.; Simas, A. M.; Longo, R. L.; Santa-Cruz, P. A.; da Silva, E. F. *Coordination Chemistry Reviews* **2000**, *196*, 165–195.

(48) Carlos, L. D.; Ferreira, R. A. S.; de Zea Bermudez, V.; Ribeiro, S. J. L. *Adv. Mater.* **2009**, *21*, 509–534.

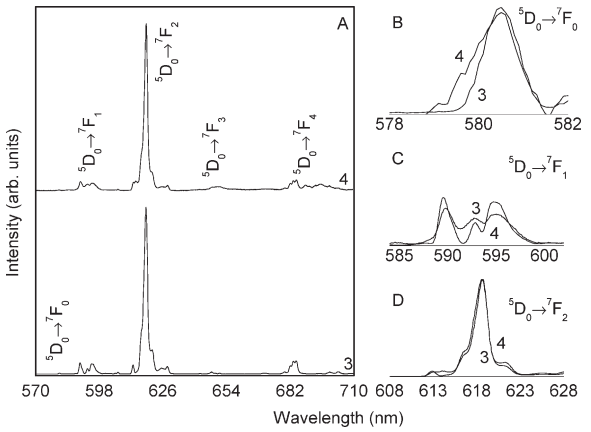

Figure 4. (A) Emission spectra acquired at 14 K for the (3) $Eu(H_2O)_5[Mo(CN)_8]$ and (4) $Eu(H_2O)_5[W(CN)_8]$ crystals excited at 395 nm. (B, C, and D) Magnifications of the $^5D_0 \rightarrow {}^7F_{0\text{-}2}$ transitions.

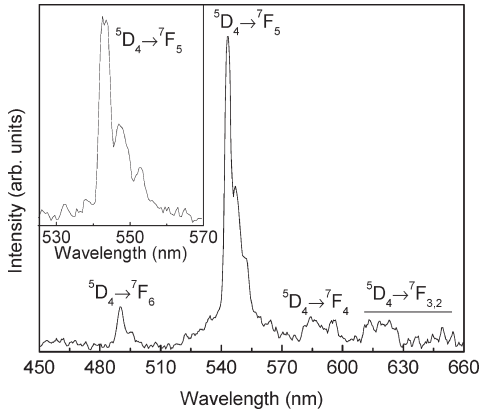

Figure 5. Emission spectra acquired at 14 K for the $Tb(H_2O)_5[W(CN)_8]$ crystals excited at 355 nm. The inset shows a magnification of the $^5D_4 \rightarrow {}^7F_5$ transition excited at 360 nm.

(with the exception of Gd^{3+}) possess a first-order angular momentum which prevents the use of a spin-only Hamiltonian for isotropic exchange.[49] For the $4f^n$ configuration of a Ln^{3+} ion, it splits into $^{2S+1}L_J$ states by interelectronic repulsion and spin−orbit coupling. Further splitting into Stark sublevels is caused by crystal-field perturbation. At high temperatures, all of the Stark levels are populated, but as the temperature decreases, the effective magnetic moment of the lanthanide ion will change as a result of thermal depopulation of the Stark sublevels.

$Eu(H_2O)_5[M(CN)_8]$ (M = Mo, W). The temperature dependences of the magnetic susceptibility, χ, and the χT product performed for both compounds with an applied field of 1000 Oe are shown in Figure 6. At 300 K, the χT values are equal to 1.79 emu K mol^{-1} and 1.80 emu K mol^{-1} for $Eu(H_2O)_5[Mo(CN)_8]$ and $Eu(H_2O)_5[W(CN)_8]$, respectively. These values are slightly lower than the calculated one of 1.875 emu K mol^{-1} for a noninteracting Eu^{3+} ion (1.5 emu K mol^{-1}) and a M^{5+} ion (0.375 emu K mol^{-1}).[50] The χT curves decrease progressively as the temperature decreases, and at 2 K, the χT values are equal to 0.007 emu K mol^{-1} and 0.006 emu K mol^{-1}, respectively. The temperature dependences of the magnetic susceptibilities, also shown in Figure 6 for both compounds,

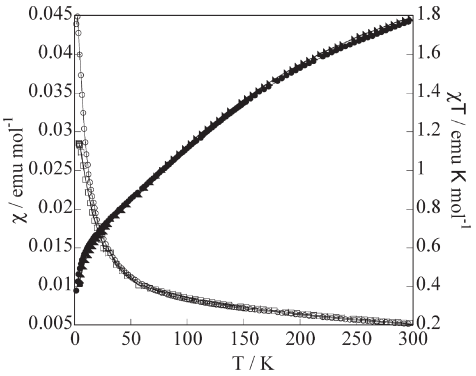

Figure 6. Temperature dependence of the magnetic susceptibility, χ, performed for $Eu(H_2O)_5[Mo(CN)_8]$ (□) and $Eu(H_2O)_5[W(CN)_8]$ (○) and the temperature dependence of the χT product for $Eu(H_2O)_5[Mo(CN)_8]$ (●) and $Eu(H_2O)_5[W(CN)_8]$ (▲) performed with an applied field of 1000 Oe.

increase as the temperature decreases, exhibiting a peak at 2.4 K. The Eu^{3+} ion has a $^7F_0$ ground state, with the first excited state $^7F_1$ at ca. 350 cm^{-1} and $^7F_2$ at ca. 1000 cm^{-1}.[51] At room temperature, these excited states are populated, but as the temperature decreases, there is a progressive depopulation of the excited doublets. At low temperatures, only the nonmagnetic ground level is occupied. In this case, the susceptibility of the isolated ion becomes temperature-independent due to field-determined admixing of the excited states into $^7F_0$.[52] Therefore, the low-temperature magnetic behavior of these compounds must be determined by the exchange interactions between the M^{5+} ions with spins equal to 1/2. The maximum observed in the temperature dependence of the susceptibility indicates that antiferromagnetic exchange interactions are operative. In order to confirm this assumption, we performed the temperature dependence of the ac susceptibility at low temperatures. For both compounds, the χ' component of the ac susceptibility shows a frequency-independent peak at 2.33 K, while the χ'' component equals zero in the measured temperature range, which confirms the presence of antiferromagnetic interactions at low temperatures.

$Tb(H_2O)_5[M(CN)_8]$ (M = Mo, W). The temperature dependences of the χT product and $1/\chi$ performed for $Tb(H_2O)_5[Mo(CN)_8]$ and $Tb(H_2O)_5[W(CN)_8]$ with an applied field of 1000 Oe are shown in Figure 7. At 300 K, the χT values of 12.12 emu K mol^{-1} and 12.19 emu K mol^{-1} observed for $Tb(H_2O)_5[Mo(CN)_8]$ and $Tb(H_2O)_5[W(CN)_8]$, respectively, correspond well to the calculated values for a noninteracting Tb^{3+} (11.75 emu K mol^{-1}) and M^{5+} (M = Mo or W; 0.37 emu K mol^{-1}) ions.[50] For both compounds, the χT decreases progressively as the temperature decreases, reaches minima values at 12 K, that is, 11.14 emu K mol^{-1} for $Tb(H_2O)_5[Mo(CN)_8]$ and 11.77 emu K mol^{-1} for $Tb(H_2O)_5[W(CN)_8]$, and then rapidly increases. The presence of minima on these curves may be attributed to the depopulation of the Stark levels of the terbium $^7F_6$ ground state as the temperature is lowered.[10,12a] Above 50 K, the temperature dependences of $1/\chi$ were fitted with

(49) Benelli, C.; Gatteschi, D. *Chem. Rev.* **2002**, *102*, 2369–2387.
(50) Carlin, R. L. *Magnetochemistry*, Springler, Berlin, 1997.
(51) Benelli, C.; Caneschi, A.; Gatteschi, D.; Pardi, L.; Rey, P. *Inorg. Chem.* **1989**, *28*, 275.
(52) King, R. B. *J. Am. Chem. Soc.* **1970**, *92*, 6455.

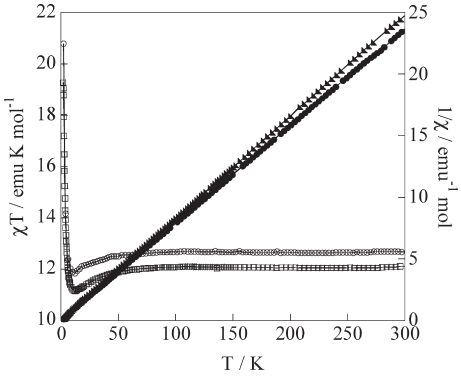

Figure 7. Temperature dependence of the χT product performed for Tb$(H_2O)_5$[Mo$(CN)_8$] (□) and Tb$(H_2O)_5$[W$(CN)_8$] (○) and the temperature dependence of the $1/\chi$ product for Tb$(H_2O)_5$[Mo$(CN)_8$] (▲) and Tb$(H_2O)_5$[W$(CN)_8$] (●) performed with an applied field of 1000 Oe.

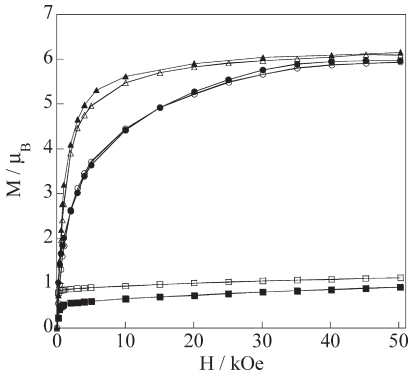

Figure 8. Field dependence of the magnetization performed at 1.8 K for Tb$(H_2O)_5$[Mo$(CN)_8$] (○), Tb$(H_2O)_5$[W$(CN)_8$] (●), Gd$(H_2O)_5$[Mo$(CN)_8$] (▽), Gd$(H_2O)_5$[W$(CN)_8$] (▲), Sm$(H_2O)_5$[Mo$(CN)_8$] (□), and Sm$(H_2O)_5$[W$(CN)_8$] (■).

the Curie−Weiss law, $1/\chi_M = (T - \Theta)/C$, with Curie constants of 12.06 emu mol^{-1} and 12.12 emu mol^{-1} and with Weiss constants of 0.27 K and 0.38 K, respectively, for Tb$(H_2O)_5$[Mo$(CN)_8$] and Tb$(H_2O)_5$[W$(CN)_8$], suggesting the presence of predominant ferromagnetic interactions.

The field dependences of the magnetization performed at 1.8 K show values of magnetization of 5.91 and 5.96 μ_B at 50 kOe for Tb$(H_2O)_5$[Mo$(CN)_8$] and Tb$(H_2O)_5$[W$(CN)_8$] (Figure 8), respectively. These values are expected for ferromagnetic interactions between Tb^{3+} and M^{5+} ions (6 μ_B) if we assume a spin of $S_M = 1/2$ with $g = 2$ for Mo^{5+} or W^{5+} ions and we take into account an approximation of an effective spin of $S = 1/2$ with strong uniaxial Ising-spin anisotropy of the **g** tensor, $g_{||} = 10$ and $g_\perp = 0$, for the Tb^{3+} ion.[50,53] This approximation is in agreement with the previously published studies in which Tb^{3+} has a similar local coordination.[12a] The presence of ferromagnetic $Tb^{3+}-Mo^{5+}$ interactions through the cyano bridge is also in accord with a previously reported cyano-bridged one-dimensional $Tb^{3+}-Mo^{5+}$ compound.[12a]

The temperature dependences of the ac susceptibility for its in-phase, χ', and out-of-phase, χ'', components performed for Tb$(H_2O)_5$[W$(CN)_8$] in a zero applied direct current (dc) field at 1 Hz show peaks at 2.10 and 2.07 K, respectively, for χ' and χ'' (Figure 9). These peaks are not frequency-dependent, which suggests the presence of a long-range magnetic ordering; on the contrary, the appearance of frequency-dependent peaks indicates the presence of a short-range ordering. The critical temperature, usually determined as the temperature at which the χ'' components became different from zero, is equal to 2.80 K for this compound. For the compound Tb$(H_2O)_5$[Mo$(CN)_8$], both χ' and χ'' responses increase dramatically above 2.3 K; however, no peaks are visible at low temperatures (insert of Figure 9), which provides some difficulty in coming to a conclusion about the presence or not of long-range magnetic ordering for this compound.

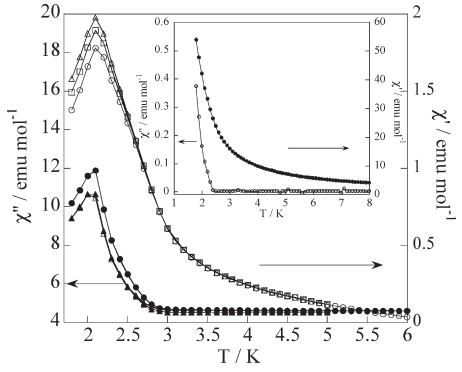

Figure 9. Temperature dependence of in-phase, χ', and out-of-phase, χ'', components of the ac susceptibility performed at 1.0, 125.0, and 999.9 Hz for Tb$(H_2O)_5$[W$(CN)_8$]. Inset: Temperature dependence of in-phase, χ', and out-of phase, χ'', components of the ac susceptibility performed at 1.0 Hz for Tb$(H_2O)_5$[Mo$(CN)_8$].

Gd$(H_2O)_5$[M$(CN)_8$] (M = Mo, W). The Gd^{3+} ion has a $^8S_{7/2}$ ground state without first-order angular momentum. The magnetic behavior of both compounds containing Gd^{3+} follows the Curie law with room-temperature χT values equal to 8.21 emu K mol^{-1} and 8.19 emu K mol^{-1} for Gd$(H_2O)_5$[Mo$(CN)_8$] and Gd$(H_2O)_5$[W$(CN)_8$], respectively. These values correspond to what is expected for noninteracting Gd^{3+} ($S = 7/2$ with ground state $^8S_{7/2}$) and M^{5+} ions (Mo or W with $S = 1/2$).[50] Below 150 K, the χT products decrease to reach minima at 27 K and 36 K for Gd$(H_2O)_5$[Mo$(CN)_8$] and Gd$(H_2O)_5$[W$(CN)_8$], respectively, then increase dramatically to reach maxima at 2.12 K and 2.15 K, respectively (Figure 10). The temperature dependences of $1/\chi$ were fitted with the Curie−Weiss law, $1/\chi_M = (T - \Theta)/C$, with Curie constants of 8.16 emu mol^{-1} and 8.07 emu mol^{-1} and with Weiss constants of −0.13 K and −0.35 K, respectively, for Gd$(H_2O)_5$[Mo$(CN)_8$] and Gd$(H_2O)_5$[W$(CN)_8$], suggesting the presence of predominant antiferromagnetic interactions. The field dependences of the magnetization performed at 1.8 K confirm for both compounds the presence of antiferromagnetic interactions between Gd^{3+} and M^{5+} through the cyano bridge, showing saturation magnetizations of 6.10 and 6.15 μ_B (the value of the saturation magnetization for antiferromagnetic $Gd^{3+}-M^{5+}$ interactions is equal to 6 μ_B, and that for ferromagnetic $Gd^{3+}-M^{5+}$ interactions is equal to 8 μ_B; Figure 8). The presence of antiferromagnetic interactions between Gd^{3+} and Mo^{5+} through the cyano bridge was

(53) (a) Evangelisti, M.; Kahn, M. L.; Bartolomé, J.; de Jongh, L. J.; Meyers, C.; Leandri, J.; Leroyer, Y.; Mathoniere, C. *Phys. Rev. B* **2003**, *68*, 2534–2549. (b) Orton, J. W. *EPR. An Introduction to Transition Group Ions in Crystals*, Gordon and Breach, New York, 1968; (c) Sen, H; Neogy, D.; Wanklyn, B. M. *J. Magn. Magn. Mater.* **1988**, *73*, 221–228.

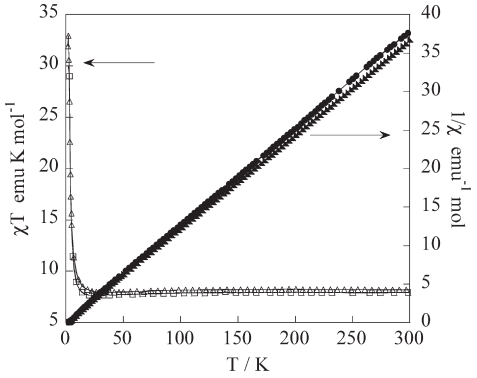

Figure 10. Temperature dependence of the χT product performed for $Gd(H_2O)_5[Mo(CN)_8]$ (□) and $Gd(H_2O)_5[W(CN)_8]$ (▽) and $1/\chi$ performed for $Gd(H_2O)_5[Mo(CN)_8]$ (●) and $Gd(H_2O)_5[W(CN)_8]$ (▲) with an applied field of 1000 Oe.

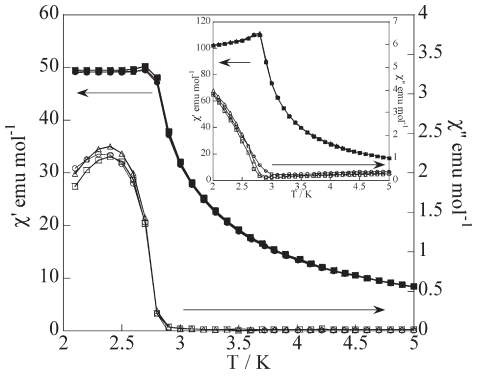

Figure 11. Temperature dependence of in-phase, χ', and out-of phase, χ'', components of the ac susceptibility for $Gd(H_2O)_5[W(CN)_8]$ with different frequencies. Inset: Temperature dependence of in-phase, χ', and out-of phase, χ'', components of the ac susceptibility for $Gd(H_2O)_5[Mo(CN)_8]$ with different frequencies. Frequencies: 1.00 Hz (■), 125 Hz (●), and 999.87 Hz (▲) for χ' and 1.00 Hz (□), 125 Hz (○), 999.87 Hz (△) for χ''.

previously reported for several one-dimensional compounds.[12c,54]

The temperature dependences of the ac susceptibility performed with different frequencies for $Gd(H_2O)_5[Mo(CN)_8]$ and $Gd(H_2O)_5[W(CN)_8]$ show an abrupt increase of χ' and χ'' responses at low temperatures. At 125 Hz, χ' shows a peak at 2.80 K and χ'' increases continuously for the first compound (Figure 11), while for the second compound, χ' and χ'' present peaks at 2.70 and at 2.3 K, respectively. These temperature dependences are non-frequency-dependent, which is indicative of the presence of a long-range magnetic ordering. The ordering temperatures determined as the temperature at which the χ'' components became different from zero are equal to 2.90 K for both compounds.

$Sm(H_2O)_5[M(CN)_8]$ (M = Mo, W). The Sm^{3+} ion has a $^6H_{5/2}$ ground state, which splits by the spin−orbit coupling into six levels. The first ($^6H_{7/2}$) and even higher excited states can be populated at room temperature. As a consequence, the high-temperature behaviour of χT vs T for the Sm^{3+} ion deviates from linearity. In addition, the presence of low-lying excited states adds a significant temperature-independent contribution to the magnetic susceptibility. Previously, it was reported by Haschimoto et al. that $Sm(H_2O)_5[W(CN)_8]$ presents peculiar magnetic behaviour showing cooling-rate-dependent ferromagnetism.[13b] The preliminary results show that, with fast cooling to low temperatures (10 K), this compound presents ferromagnetic behavior with a long-range magnetic ordering at 2.8 K, while ferrimagnetism with a Néel temperature of 3 K was obtained with slow cooling of the sample (the cooling rate being 1 K min^{-1}). This phenomenon was attributed to the overcooling effect of the structural phase transition occurring at 166 K. The magnetic measurements on our $Sm(H_2O)_5[Mo(CN)_8]$ and $Sm(H_2O)_5[W(CN)_8]$ samples were performed by fast cooling of the samples to 10 K. The temperature dependences of the χT product and $1/\chi$ performed for $Sm(H_2O)_5[Mo(CN)_8]$ and $Sm(H_2O)_5[W(CN)_8]$ with an applied field of 1000 Oe are shown in Figure 12. At 300 K, the χT values are equal to 0.49 emu K mol^{-1} and 0.53 emu K mol^{-1} for the first and second compounds, respectively. These values are in good agreement

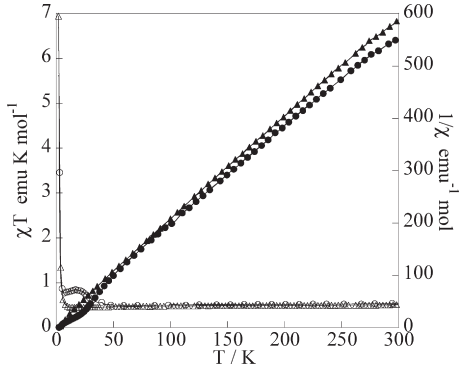

Figure 12. Temperature dependence of the χT product performed for $Sm(H_2O)_5[Mo(CN)_8]$ (▽) and $Sm(H_2O)_5[W(CN)_8]$ (○) and $1/\chi$ performed for $Sm(H_2O)_5[Mo(CN)_8]$ (■) and $Sm(H_2O)_5[W(CN)_8]$ (●) with an applied field of 1000 Oe.

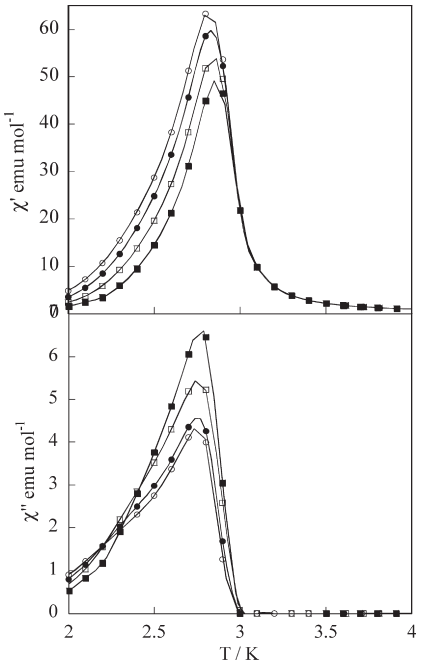

Figure 13. Temperature dependence of in-phase, χ' (top), and out-of phase, χ'' (bottom), components of the ac susceptibility performed at 1.00 Hz (○), 9.99 Hz (●), 125.00 Hz (□), and 999.87 Hz (■) for $Sm(H_2O)_5[Mo(CN)_8]$.

(54) Przychodzen, P.; Pełka, R.; Lewiński, K.; Supel, J.; Rams, M.; Tomala, K.; Sieklucha, B. *Inorg. Chem.* **2007**, *46*, 8924–8938.

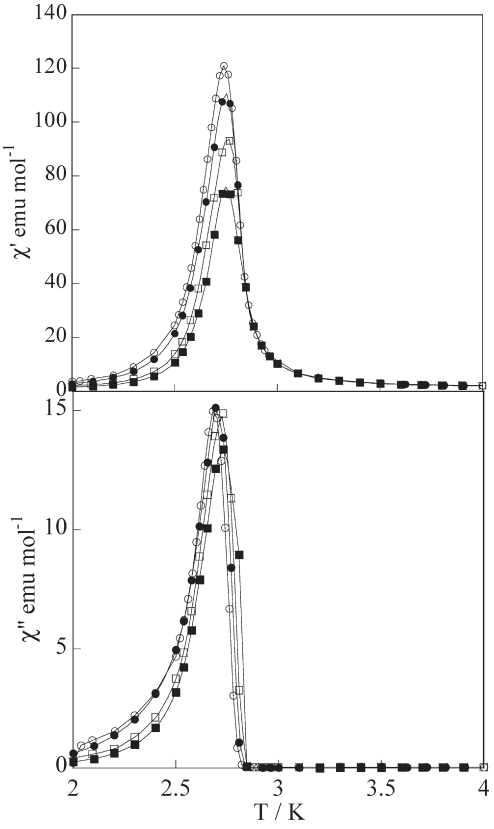

Figure 14. Temperature dependence of in-phase, χ' (top), and out-of phase, χ'' (bottom), components of the ac susceptibility performed by fast cooling at 1.00 Hz (□), 9.99 Hz (▲), 125.00 Hz (●), 997.34 Hz (○), and 1488.10 Hz (■) for $Sm(H_2O)_5[W(CN)_8]$.

with the values previously observed for the one-dimensional $Sm^{3+}-Mo^{5+}$ and two-dimensional $Sm^{3+}-W^{5+}$ compounds.[54,13b] For $Sm(H_2O)_5[Mo(CN)_8]$, the χT value decreases slowly as the temperature decreases, reaches a minimum at 16.07 K, and then increases rapidly, reaching the maximum value at 1.83 K. The χT vs T curve of $Sm(H_2O)_5[W(CN)_8]$ presents a minimum at 30.73 K, then increases, reaches a maximum at 18.7 K, decreases slowly, and increases again, reaching a maximum value at 2.3 K as the temperature decreases. As for the Tb^{3+}-containing compounds, the presence of the minima on these curves may be attributed to the depopulation of the Stark levels of the samarium ground state.[50]

The field dependences of the magnetization performed at 1.8 K show values of the saturation magnetization of 0.91 and 0.95 μ_B (at 50 kOe) for $Sm(H_2O)_5[Mo(CN)_8]$ and $Sm(H_2O)_5[W(CN)_8]$ (Figure 8) with weak coercive fields of 25 and 65 Oe, respectively. These values of the saturation magnetization are low in comparison to the expected value for ferromagnetic interactions between Sm^{3+} and Mo^{5+} or W^{5+}, which should be equal to 1.71 μ_B, but much higher in comparison to the calculated value for antiferromagnetic interactions, which should be equal to 0.29 μ_B.[50] Close values of the saturation magnetization (around 0.91 μ_B) were obtained for one- and two-dimensional $Sm^{3+}-W^{5+}$ compounds and were attributed to the presence of ferromagnetic interactions between Sm^{3+} and W^{5+} ions through the cyano bridge.[13b,54] The weak values of the saturation magnetization in comparison with the calculated one were explained by the fact that, at 1.8 K, the full saturation cannot be reached due to the low value of the ordering temperature.

The temperature dependence of the ac susceptibility performed for $Sm(H_2O)_5[Mo(CN)_8]$ shows that both χ' and χ'' responses present non-frequency-dependent peaks at 2.83 and 2.77 K, suggesting the occurrence of a long-range magnetic transition (Figure 13). The critical temperature determined as the temperature at which the χ'' components became different from zero is equal to 3.00 K. Similar behavior was observed for $Sm(H_2O)_5[W(CN)_8]$. Its temperature dependence for the χ' and χ'' responses presents non-frequency-dependent peaks at 2.73 and 2.69 K, respectively, with a long-range magnetic ordering critical temperature at 2.84 K (Figure 14).

Conclusion

In summary, we report here the synthesis, structure, photoluminescence, and magnetic characterization of eight new two-dimensional cyano-bridged coordination polymers $Ln(H_2O)_5[M(CN)_8]$ (where Ln = Eu, Tb, Sm, Gd and M = Mo, W). These compounds are isomorphous and crystallize in the tetragonal system *P*4/*nmm* in order to form two-dimensional gridlike networks. The Eu- and Tb-containing coordination polymers exhibit the typical intra-4f lines ascribed to the $^5D_0 \rightarrow {}^7F_{0-4}$ (Eu^{3+}) and $^5D_4 \rightarrow {}^7F_{6-2}$ (Tb^{3+}) transitions. The O → W and O → Eu LMCT states were discerned at 257 and 270 nm, respectively. Except for the $Tb(H_2O)_5[W(CN)_8]$ crystal for which the O → W LMCT path dominates, the Ln^{3+} sensitization occurs mainly via direct intra-4f excitation. The $^5D_0$ and $^5D_4$ lifetime values (under direct intra-4f excitation) in the W^{5+}-containing crystals are smaller than those containing Mo^{5+}, which may indicate a higher nonradiative transition probability for the former materials. Investigations of the magnetic properties of these compounds show the presence of low-temperature magnetic ordering for all compounds except Eu-containing coordination polymers because Eu^{3+} is diamagnetic at low temperatures. Thus, while $Eu(H_2O)_5[M(CN)_8]$ presents antiferromagnetic interactions between the M^{5+} ions through CN−Eu−NC units, $Tb(H_2O)_5[M(CN)_8]$ and $Sm(H_2O)_5[M(CN)_8]$ display ferromagnetic and $Gd(H_2O)_5[M(CN)_8]$ displays antiferromagnetic $Ln^{3+}-M^{5+}$ interactions through the cyano-bridge. The nonluminescent $Sm(H_2O)_5[M(CN)_8]$ and $Gd(H_2O)_5[M(CN)_8]$ present magnetic ordering at low temperatures below ca. 3 K. The $Tb(H_2O)_5[W(CN)_8]$ crystal presents long-range magnetic ordering below 2.8 K, and the presence of luminescence along with ferromagnetic ordering suggest that this compound may be identified as a bifunctional coordination polymer, exhibiting diverse physical responses when subjected to various external stimuli. Although the eventual interdependence between magnetic ordering and luminescence was not addressed in this work (due to technical difficulties associated with measuring in situ the emission at 2−3 K under an applied magnetic field), the characterization of an eventual synergy between the two functionalities is indubitably a further step towards multifunctionality. Advanced studies in similar coordination polymers are now in progress, endeavoring the design of materials with magnetic ordering at higher temperatures (> 4.2 K, at least).

Acknowledgment. The authors thank Mme. Corine Rebeil (UM2, Institute Charles Gerhardt Montpellier, France) for magnetic measurements and Dr. Kevin Bernot (INSTM, University of Florence, Italy) for discussion. The authors are grateful to *Fundação para a Ciência e a Tecnologia* (FCT, Portugal) for the financial support toward the purchase of the single-crystal diffractometer and funding (PPCDT/QUI/58377/2004). The authors also wish to thank CRUP-PAUILF (Portugal−France bi-lateral programme), CNRS, the Université Montpellier II, and networks of excellence MAGMANet and FAME for financial support.

Supporting Information Available: A crystallorgraphic file in CIF format.This material is available free of charge via the Internet at http://pubs.acs.org. Crystallographic data (excluding structure factors) for the structures reported in this paper have been deposited with the Cambridge Crystallographic Data Centre (CCDC deposition numbers are supplied in Table 1 for each structure). Copies of the data can be obtained free of charge on application to CCDC, 12 Union Road, Cambridge CB2 2EZ, U.K. FAX: (+44) 1223 336033. E-mail: deposit@ccdc.cam.ac.uk.